Shizhen Yin
State Key Laboratory of Nonlinear Mechanics,
Institute of Mechanics,
Chinese Academy of Sciences,
Beijing 100190, China;
School of Engineering Science,
University of Chinese Academy of Sciences,
Beijing 100049, China
e-mail: yinshizhen@imech.ac.cn

Yewang Su[1]
State Key Laboratory of Nonlinear Mechanics,
Institute of Mechanics,
Chinese Academy of Sciences,
Beijing 100190, China;
School of Engineering Science,
University of Chinese Academy of Sciences,
Beijing 100049, China;
Beijing Key Laboratory of Engineered Construction and Mechanobiology,
Institute of Mechanics, Chinese Academy of Sciences,
Beijing 100190, China
e-mail: yewangsu@imech.ac.cn

A Traction-Free Model for the Tensile Stiffness and Bending Stiffness of Laminated Ribbons of Flexible Electronics

Laminated ribbons have been widely adopted for structures of flexible electronics to simultaneously achieve the electronic functions and mechanical performances. Their effective tensile stiffness and bending stiffness, which are extensively used as fundamental parameters in the mechanical analysis, are usually obtained by the plane-strain hypothesis for simplicity. However, it is found that the practical condition is usually closer to the traction free, even for the cases with a relatively large width. Here, a traction-free model is proposed to analytically obtain the effective tensile stiffness and bending stiffness of laminated ribbons, which can be used directly in the mechanical analysis of flexible electronics. The prediction of the traction-free model agrees very well with the precise result obtained by 3D finite element analysis (FEA) for the cases that are in the range of structure designs of flexible electronics. It is found that the tensile/bending stiffness of traction-free model is between the plane-stress model and plane-strain model, but is closer to the plane-stress model. The use of the plane-strain model sometimes may yield a considerable error in the mechanical analysis of flexible electronics. The parameter study shows that this model is very important for the problems with advanced materials, such as metamaterials with negative Poisson's ratio. This work provides a theoretical basis for the mechanical analysis of flexible electronics. [DOI: 10.1115/1.4042920]

Keywords: laminated ribbon, tensile stiffness, bending stiffness, plane-strain, plane-stress, flexible electronics

1 Introduction

Flexible electronics have attracted increasing interest in the last decade due to its great potential applications [1,2]. Examples include electronic eye cameras [3], stretchable electronic skin [4–6], flexible health monitoring system [7–10], stretchable batteries [11], multifunctional integumentary cardiac membranes [12,13], piezoelectric energy harvesters [14–18], smart gloves for gesture recognition, and smart clothing for sitting posture monitoring [19]. More and more studies turn to practical applications [19–21] from ideal concepts of flexible electronics [22–27]. Compared with organic devices, inorganic flexible electronics may achieve practical application earlier because of their high electronic performance and proven industrial production lines.

Mechanical structural designs, analysis, and optimization are critical for the flexibility and stretchability of inorganic electronics [28–30]. The most popular stretchable structure design is the island-bridge mesh structure, as shown in Fig. 1, in which the functional components reside on the islands and are connected by the stretchable interconnects. The islands do not significantly deform, while the interconnects provide the stretchability for the entire system that is subjected to apparently applied stretch. The geometric design of the interconnects (i.e., bridges) has been developed from straight [31,32] to curved [33–35] and fractal-inspired [11,21,36,37] layouts; the initial regime of the interconnects has been developed from two-dimensional [6] to three-dimensional configurations [38]; and the deformation mechanism has been developed from buckling [39] to nonbuckling [20]. The stretchability can achieve as large as several hundred percent. For some applications that demand only the bendability rather than stretchability, thin-film-like structures are widely adopted [14,17]. The thickness of the structure is the key of the design. According to mechanical analysis, thinner structures usually have better bendability while other parameters are kept constant.

Laminated ribbons consisting of metals and polymers are widely adopted to simultaneously realize the electronic functions and mechanical bendability and stretchability (Fig. 1) [39–41]. These laminated ribbons are usually subjected to loads of tension and bending. Their effective tensile stiffness and bending stiffness, which are frequently used as fundamental parameters in the mechanical analysis, are usually obtained by the plane-strain hypothesis [14,15,17,39–44]. With this assumption, the strain along the out-of-plane direction (x direction in Fig. 2(*a*)) is zero for all layers. The reason for using the plane-strain hypothesis is sometimes just for simplicity, or that the width of the ribbon is relatively large. However, the condition of the large width does not ensure the condition of zero strain or zero stress in the x direction for all layers. The practical condition in the out-of-plane direction is usually closer to that of the apparent traction force and moment (f_x and m_x in Fig. 2(*a*)) at the two edges perpendicular to the x axis are zero, even for the cases with a relatively large width. Therefore, the mechanical condition is neither plane strain nor plane stress, but should be apparently traction free. With the condition of traction free, the interaction between each layer should be quantitatively considered. The detailed analysis will be given in the following Secs. 2 and 3.

In this paper, a traction-free model that is different from both the plane-strain model and the plane-stress model is developed to obtain the effective tensile stiffness and bending stiffness of laminated ribbons, which are frequently used in the mechanical analysis

[1]Corresponding author.

Contributed by the Applied Mechanics Division of ASME for publication in the Journal of Applied Mechanics. Manuscript received January 26, 2019; final manuscript received February 17, 2019; published online March 16, 2019. Assoc. Editor: Yong Zhu.

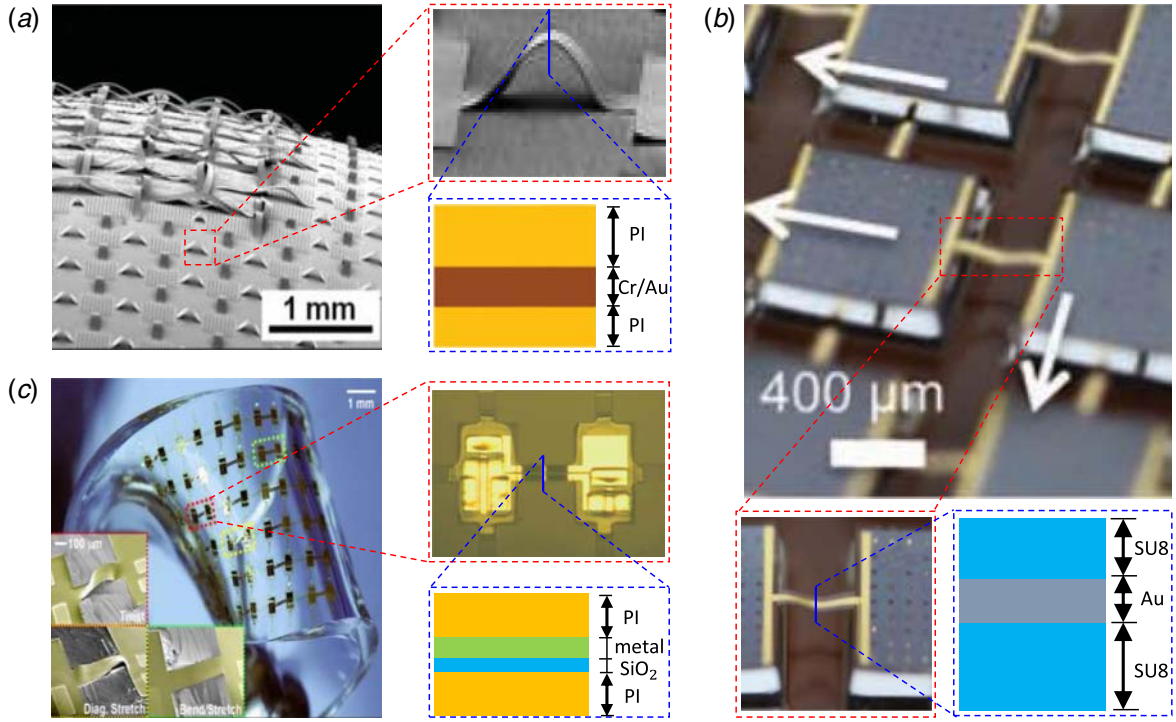

Fig. 1 Schematics of the island-bridge mesh structure of flexible electronics with laminated ribbons for interconnects (with permissions): (*a*) a four-layer ribbon consisting of PI/Cr/Au/PI, (*b*) a three-layer ribbon consisting of SU8/Au/SU8, and (c) a four-layer ribbon consisting of PI/metal/SiO_2/PI

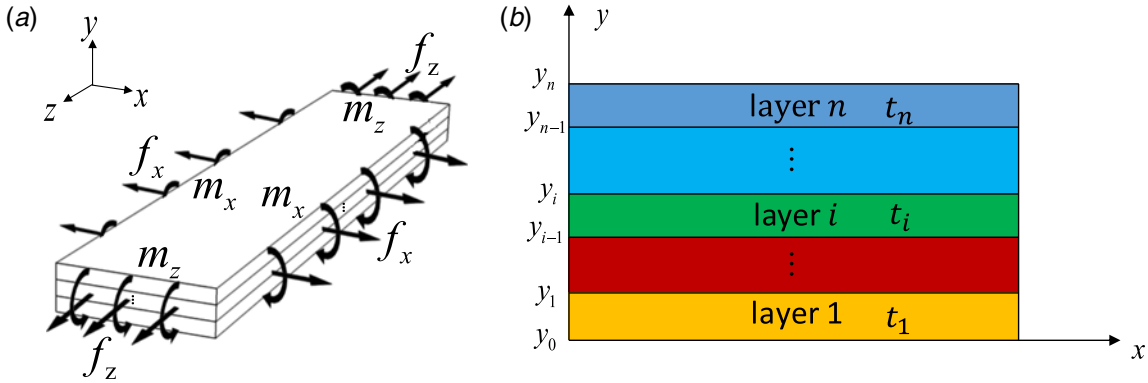

Fig. 2 (*a*) Schematic illustration of a laminated ribbon subjected to the distributed axial forces and bending moments and (*b*) the cross section of the laminated ribbon

of flexible electronic. In Sec. 2, the traction-free model is described and analyzed. Effective tensile stiffness and bending stiffness are analytically obtained. The plane-strain model and the plane-stress model are also analyzed for comparison. In Sec. 3, the traction-free model, the plane-strain model, and the plane-stress model are systematically compared with a double-layer example. Finally, concluding remarks are given in Sec. 4.

2 Analytic Models for Laminated Ribbons

In this section, a traction-free model is proposed to analyze the mechanical behaviors of laminated ribbons. The effective tensile stiffness and bending stiffness are analytically obtained by this model. As illustrated in Fig. 2(*a*), a laminated ribbon of n layers is subjected to the uniformly distributed axial forces f_x and f_z and bending moments m_x and m_z at the boundaries. The relation between the thickness t_i of each layer and the coordinate y_i is $t_i = y_i - y_{i-1}$, as shown in Fig. 2(*b*). With the loads of tension and bending, the principal strains are along the directions of the coordinates. The strains can be obtained by the Kirchhoff assumption as

$$\begin{cases} \varepsilon_x = \varepsilon_{x0} + \kappa_x \left(y - \frac{1}{2}\sum_{j=1}^{n} t_j \right) \\ \varepsilon_z = \varepsilon_{z0} + \kappa_z \left(y - \frac{1}{2}\sum_{j=1}^{n} t_j \right) \end{cases} \tag{1}$$

where ε_{x0} and ε_{z0} are the membrane strain at the middle plane ($y = \sum_{j=1}^{n} t_j/2$) of the laminate ribbon along x and z directions and κ_x and κ_z are the curvatures, respectively. It is worth noting that the middle plane need not necessarily be the neutral plane for the laminated ribbons with multiple materials, i.e., ε_{x0} and

ε_{z0} are not necessarily zero. The linear elastic constitutive relation gives the normal stresses as

$$\begin{cases} \sigma_x = \dfrac{E}{1-\nu^2}(\varepsilon_x + \nu\varepsilon_z) \\ \sigma_z = \dfrac{E}{1-\nu^2}(\varepsilon_z + \nu\varepsilon_x) \end{cases} \tag{2}$$

Here, E is Young's modulus and ν is Poisson's ratio. Therefore, the axial forces and bending moments per unit length can be obtained by integration over the entire thickness of the laminated ribbons as follows:

$$\begin{aligned} f_x &= \int_{y_0}^{y_n} \sigma_x dy \\ f_z &= \int_{y_0}^{y_n} \sigma_z dy \\ m_x &= \int_{y_0}^{y_n} \sigma_x \left(y - \frac{1}{2}\sum_{j=1}^{n} t_j \right) dy \\ m_z &= \int_{y_0}^{y_n} \sigma_z \left(y - \frac{1}{2}\sum_{j=1}^{n} t_j \right) dy \end{aligned} \tag{3}$$

Substitution of Eqs. (1) and (2) into Eq. (3) gives the relation between the axial forces/bending moments and the membrane strains/curvatures as

$$\begin{bmatrix} f_x \\ f_z \\ m_x \\ m_z \end{bmatrix} = \begin{bmatrix} \alpha_1 & \alpha_2 & \alpha_3 & \alpha_4 \\ \alpha_2 & \alpha_1 & \alpha_4 & \alpha_3 \\ \alpha_3 & \alpha_4 & \alpha_5 & \alpha_6 \\ \alpha_4 & \alpha_3 & \alpha_6 & \alpha_5 \end{bmatrix} \begin{bmatrix} \varepsilon_{x0} \\ \varepsilon_{z0} \\ \kappa_x \\ \kappa_z \end{bmatrix} \tag{4}$$

where

$$\begin{aligned} \alpha_1 &= \sum_{i=1}^{n} \frac{E_i t_i}{1-\nu_i^2} \\ \alpha_2 &= \sum_{i=1}^{n} \frac{\nu_i E_i t_i}{1-\nu_i^2} \\ \alpha_3 &= \sum_{i=1}^{n} \frac{E_i t_i}{2(1-\nu_i^2)} \left(\sum_{j=1}^{i-1} t_j + \sum_{j=1}^{i} t_j - \sum_{j=1}^{n} t_j \right) \\ \alpha_4 &= \sum_{i=1}^{n} \frac{\nu_i E_i t_i}{2(1-\nu_i^2)} \left(\sum_{j=1}^{i-1} t_j + \sum_{j=1}^{i} t_j - \sum_{j=1}^{n} t_j \right) \\ \alpha_5 &= \sum_{i=1}^{n} \frac{E_i}{3(1-\nu_i^2)} \left\{ \left[\left(\sum_{j=1}^{i} t_j - \frac{1}{2}\sum_{j=1}^{n} t_j \right)^3 - \left(\sum_{j=1}^{i-1} t_j - \frac{1}{2}\sum_{j=1}^{n} t_j \right)^3 \right] \right\} \\ \alpha_6 &= \sum_{i=1}^{n} \frac{\nu_i E_i}{3(1-\nu_i^2)} \left\{ \left[\left(\sum_{j=1}^{i} t_j - \frac{1}{2}\sum_{j=1}^{n} t_j \right)^3 - \left(\sum_{j=1}^{i-1} t_j - \frac{1}{2}\sum_{j=1}^{n} t_j \right)^3 \right] \right\} \end{aligned} \tag{5}$$

Here, E_i, ν_i, and t_i are Young's modulus, Poisson's ratio, and the thickness of the ith layer in the laminated structure, respectively. With the traction-free condition at the boundaries that is perpendicular to the x axis

$$f_x = m_x = 0 \tag{6}$$

and the zero bending moment condition

$$m_z = 0 \tag{7}$$

the tensile stiffness is obtained as

$$\begin{aligned} \overline{EA}_{z,traction-free} &= \frac{f_z}{\varepsilon_{z0}} \\ &= \frac{(\alpha_1\alpha_5 + \alpha_2\alpha_6 - \alpha_3^2 - \alpha_4^2)^2 - (\alpha_1\alpha_6 + \alpha_2\alpha_5 - 2\alpha_3\alpha_4)^2}{\alpha_1(\alpha_5^2 - \alpha_6^2) - \alpha_5(\alpha_3^2 + \alpha_4^2) + 2\alpha_3\alpha_4\alpha_6} \end{aligned} \tag{8}$$

With the traction-free conditions (6) and the zero force condition

$$f_z = 0 \tag{9}$$

the bending stiffness is obtained as

$$\begin{aligned} \overline{EI}_{z,traction-free} &= \frac{m_z}{\kappa_z} \\ &= \frac{(\alpha_1\alpha_5 + \alpha_2\alpha_6 - \alpha_3^2 - \alpha_4^2)^2 - (\alpha_1\alpha_6 + \alpha_2\alpha_5 - 2\alpha_3\alpha_4)^2}{\alpha_5(\alpha_1^2 - \alpha_2^2) - \alpha_1(\alpha_3^2 + \alpha_4^2) + 2\alpha_2\alpha_3\alpha_4} \end{aligned} \tag{10}$$

In the plane-strain model, $\varepsilon_x = \varepsilon_{x0} + \kappa_x\left(y - \sum_{j=1}^{n} t_j/2\right) = 0$ is required. The traction-free model can be degenerated to the plane-strain model by applying the condition

$$\varepsilon_{x0} = \kappa_x = 0 \tag{11}$$

to the above derivations. In conventional derivation of plane-strain tensile stiffness, the effect of bending is not considered. By applying the additional condition $\kappa_z = 0$, the tensile stiffness of the plane-strain model can be obtained as

$$\overline{EA}_{z,plane-strain} = \alpha_1 = \sum_{i=1}^{n} \frac{E_i t_i}{1-\nu_i^2} \tag{12}$$

With the traction-free condition (11), the bending stiffness then degenerates to

$$\overline{EI}_{z,plane-strain} = \alpha_5 - \frac{\alpha_3^2}{\alpha_1} \tag{13}$$

Replacing $E_i/(1-\nu_i^2)$ by E_i, in Eqs. (5), (12), and (13), the tensile stiffness and bending stiffness for the plane-stress model are obtained as

$$\overline{EA}_{z,plane-stress} = \alpha_1' = \sum_{i=1}^{n} E_i t_i \tag{14}$$

and

$$\overline{EI}_{z,plane-strain} = \alpha_5' - \frac{(\alpha_3')^2}{\alpha_1'} \tag{15}$$

where

$$\begin{aligned} \alpha_1' &= \sum_{i=1}^{n} E_i t_i \\ \alpha_3' &= \sum_{i=1}^{n} \frac{E_i t_i}{2} \left(\sum_{j=1}^{i-1} t_j + \sum_{j=1}^{i} t_j - \sum_{j=1}^{n} t_j \right) \\ \alpha_5' &= \sum_{i=1}^{n} \frac{E_i}{3} \left\{ \left[\left(\sum_{j=1}^{i} t_j - \frac{1}{2}\sum_{j=1}^{n} t_j \right)^3 - \left(\sum_{j=1}^{i-1} t_j - \frac{1}{2}\sum_{j=1}^{n} t_j \right)^3 \right] \right\} \end{aligned} \tag{16}$$

There are two special cases that should be discussed here:

(1) For $\nu_i = \nu$, Poisson's ratio of each layer is the same. The coefficient α_i in Eq. (5) degenerates to

$$\alpha_1 = \frac{1}{1-\nu^2}\alpha_1', \quad \alpha_2 = \frac{\nu}{1-\nu^2}\alpha_1', \quad \alpha_3 = \frac{1}{1-\nu^2}\alpha_3', \quad \alpha_4 = \frac{\nu}{1-\nu^2}\alpha_3', \quad \alpha_5 = \frac{1}{1-\nu^2}\alpha_5', \quad \alpha_6 = \frac{\nu}{1-\nu^2}\alpha_5' \tag{17}$$

The bending stiffness of traction-free model given in Eq. (10) degenerates to Eq. (15) that is for the plane-stress model. Similar to the derivation of Eq. (8), the tensile stiffness of the traction-free model degenerates to Eq. (14) that is for the plane-stress model, by the application of the additional condition $\kappa_z = 0$.

(1) For $\nu_i = 0$, Poisson's ratio of each layer is zero. The coefficient α_i in Eq. (5) degenerates to

$$\alpha_1 = \frac{1}{1-\nu^2}\alpha_1', \quad \alpha_2 = 0, \quad \alpha_3 = \frac{1}{1-\nu^2}\alpha_3', \quad \alpha_4 = 0, \quad \alpha_5 = \frac{1}{1-\nu^2}\alpha_5', \quad \alpha_6 = 0 \tag{18}$$

The bending stiffness of the three models becomes exactly the same. With the application of the additional condition $\kappa_z = 0$ to the traction-free model, the tensile stiffness of the three models also agrees with each other.

3 Results and Discussions

In this section, the traction-free model, the plane-strain model, and the plane-stress model are compared systematically with an example of a double-layer ribbon. The underlying mechanism that yields the difference among the models is investigated. Effects of the parameters, such as the width of the ribbon, Young's modulus, and Poisson's ratio on the tensile stiffness and the bending stiffness are studied comprehensively. Finite element analysis (FEA) with three-dimensional (3D) practical conditions is conducted to verify the results.

The cross section of the double-layer ribbon with width w, thickness t_i, Young's modulus E_i, and Poisson's ratio ν_i for the ith layer is shown in Fig. 3(*a*). To study the tensile stiffness, a uniformly distributed tensile force f_z is applied to the two ends of the ribbon while other forces and moments are zero (Fig. 2(*a*)). For the bending stiffness, a uniformly distributed bending moment m_z is applied to the two ends of the ribbon, while other forces and moments are zero (Fig. 2(*a*)). With the thicknesses $t_1 = t_2 = 1\ \mu$m,

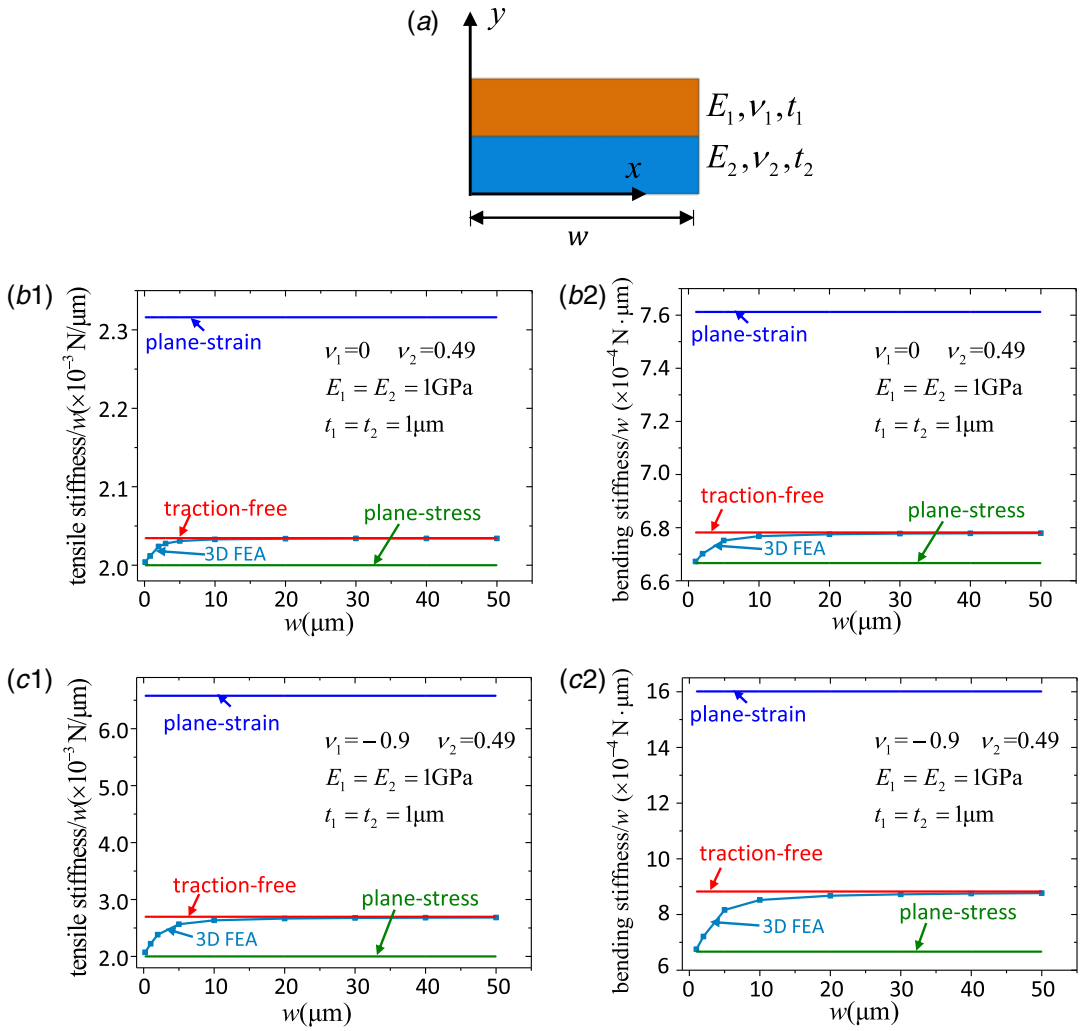

Fig. 3 (*a*) **Schematic illustration of the cross section of the double-layer ribbon. Comparison of the tensile/bending stiffness of the three models and 3D FEA, and the effects of the width: (*b*1) $\nu_1 = 0$, $\nu_2 = 0.49$ for tensile stiffness, (*b*2) $\nu_1 = 0$, $\nu_2 = 0.49$ for bending stiffness, (c1) $\nu_1 = -0.9$, $\nu_2 = 0.49$ for tensile stiffness, and (c2) $\nu_1 = -0.9$, $\nu_2 = 0.49$ for bending stiffness.**

Young's moduli $E_1 = E_2 = 1$ GPa and Poisson's ratios $\nu_1 = 0, \nu_2 = 0.49$, the comparison of tensile/bending stiffness of the three models and the effects of the width w are depicted in Figs. 3(*b*1) and 3(*b*2), respectively. For all the ranges of the width w, the tensile/bending stiffness per width of the traction-free model is between that of the plane-stress model and the plane-strain model. The precise result predicted by FEA (see the next paragraph for detail) verified the traction-free model. For $w > 10$ μm that is in the range of structure designs of flexible electronics, the tensile/bending stiffness resulting from the traction-free model agrees very well with the FEA prediction, while the precise result approaches the plane-stress model for the narrower width w. For a small width w, the deformation mode of most regions does not follow the Kirchhoff assumption, and the result of 3D FEA for practical conditions deviates from the traction-free model and approaches that of the plane-stress model. Moreover, the result of the traction-free model is closer to that of the plane-stress model, instead of the plane-strain model that has been usually adopted in the past mechanical analysis for simplicity [14,15]. With the development of material science, metamaterials with extreme mechanical properties are widely utilized in advanced structures and devices. In this context, the case with $\nu_1 = -0.9$ and $\nu_2 = 0.49$ is studied in Figs. 3(*c*1) and 3(*c*2). The tensile/bending stiffness of the plane-strain model is more than three/two times as large as that of the plane-stress model, while the traction-free model is closer to the plane-stress model.

In the model of FEA, the 3D solid element with real dimensions and material parameters is used to simulate the practical conditions. The stress-free condition is applied at the two edges perpendicular to the x axis (Fig. 2(*a*)), as well as the bottom and top surfaces. Because the tensile/bending stiffness should be independent of the length of the model, the hypothesis of the plane section is kept at the two edges perpendicular to the z axis (Fig. 2(*a*)) by using of the "reference point," the "rigid plane," and the "nonfriction contact" in the commercial software ABAQUS [45]. With these conditions, the hypothesis of the plane section (x–y plane) is kept everywhere along the z axis, while the interaction between adjacent layers appears along the x axis.

To understand the underlying mechanism that yields the difference among the three models, the distribution of the shear stress τ_{xy} at the interface between the two layers is studied with the example of the tension of the double-layer ribbon. For the plane-strain model, there is no shear stress τ_{xy} at the interface between adjacent layers, which is ensured by the condition of zero strain ε_{xx} for each layer. The "constraint" along the x direction is very "strong." In the plane-stress model, the condition of zero stress σ_{xx} is confirmed, and the deformation in x direction is free and independent for each layer. Shear stress τ_{xy} is also zero or not considered in fact. The "constraint" along the x direction is "zero." In the traction-free model, the condition of zero traction force and moment is ensured anywhere along the x axis, while shear stress between the adjacent layers locates near the two boundaries as shown in Fig. 4. The "constraint" along the x direction is very "weak." The order of the "constraint" of the three models corresponds to the order of the amplitude of the tensile stiffness, as shown in Figs. 3(*b*1), 3(*b*2), 3(*c*1), and 3(*c*2). Figure 4(*a*) shows the distribution of the shear stress τ_{xy} normalized by the applied stress σ_{zz} obtained by the 3D FEA with practical conditions. For a small width ($w < \sim 3$ μm), the shear stress distributes in the entire width and the peak is relatively small. The traction-free model approaches the plane-stress model, which is confirmed by the 3D FEA (Fig. 3). For a larger width ($w > \sim 3$ μm), the nonzero shear stress distributes mainly at the area near the two boundaries. This point is further shown in Fig. 4(*b*). The shear stress τ_{xy} transfers and balances the normal stress σ_{xx} of the two layers in a transferring region with the size of $r_{transfer}$. When the width w reaches a certain large value, the peak of shear stress becomes a constant $\tau_{\max}$, which is independent of the width w. The transferring region $r_{transfer}$ can be defined as the size of the region where $\tau_{xy}/\tau_{\max} \geq 1\%$. As shown in Fig. 4(*b*), $r_{transfer}$ increases with the increase in the width w at the

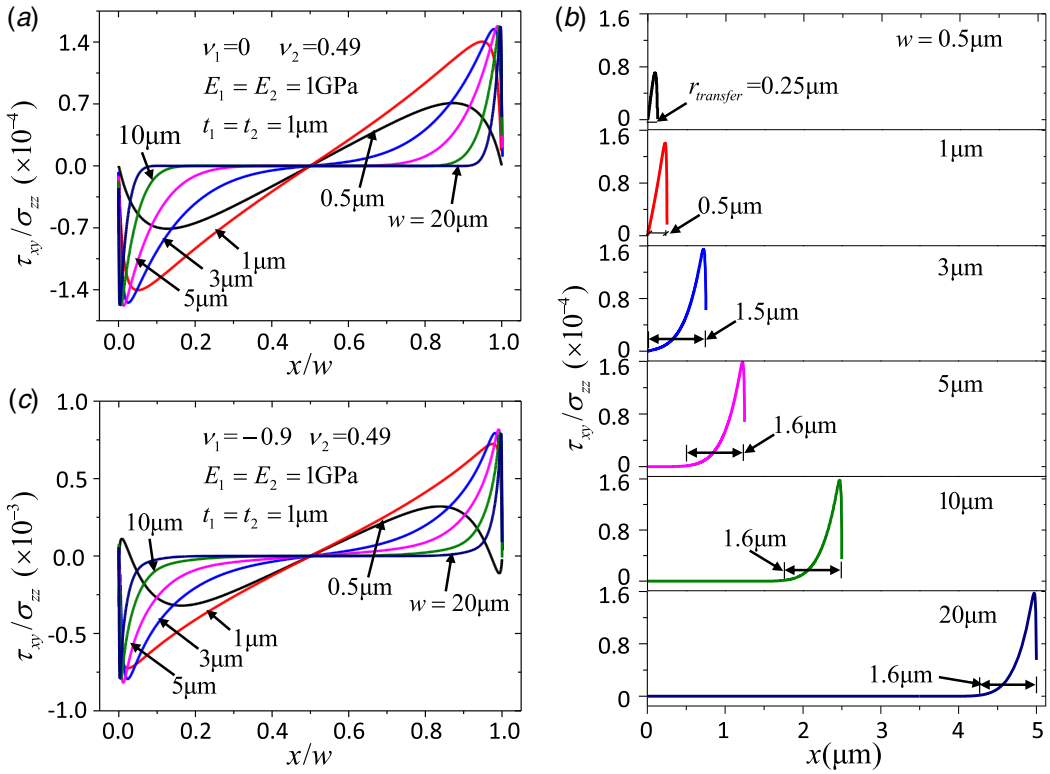

Fig. 4 The distribution of the normalized shear stress at the interface between the two layers along the *x* axis: (*a*, *b*) $\nu_1 = 0$ and (*c*) $\nu_1 = -0.9$

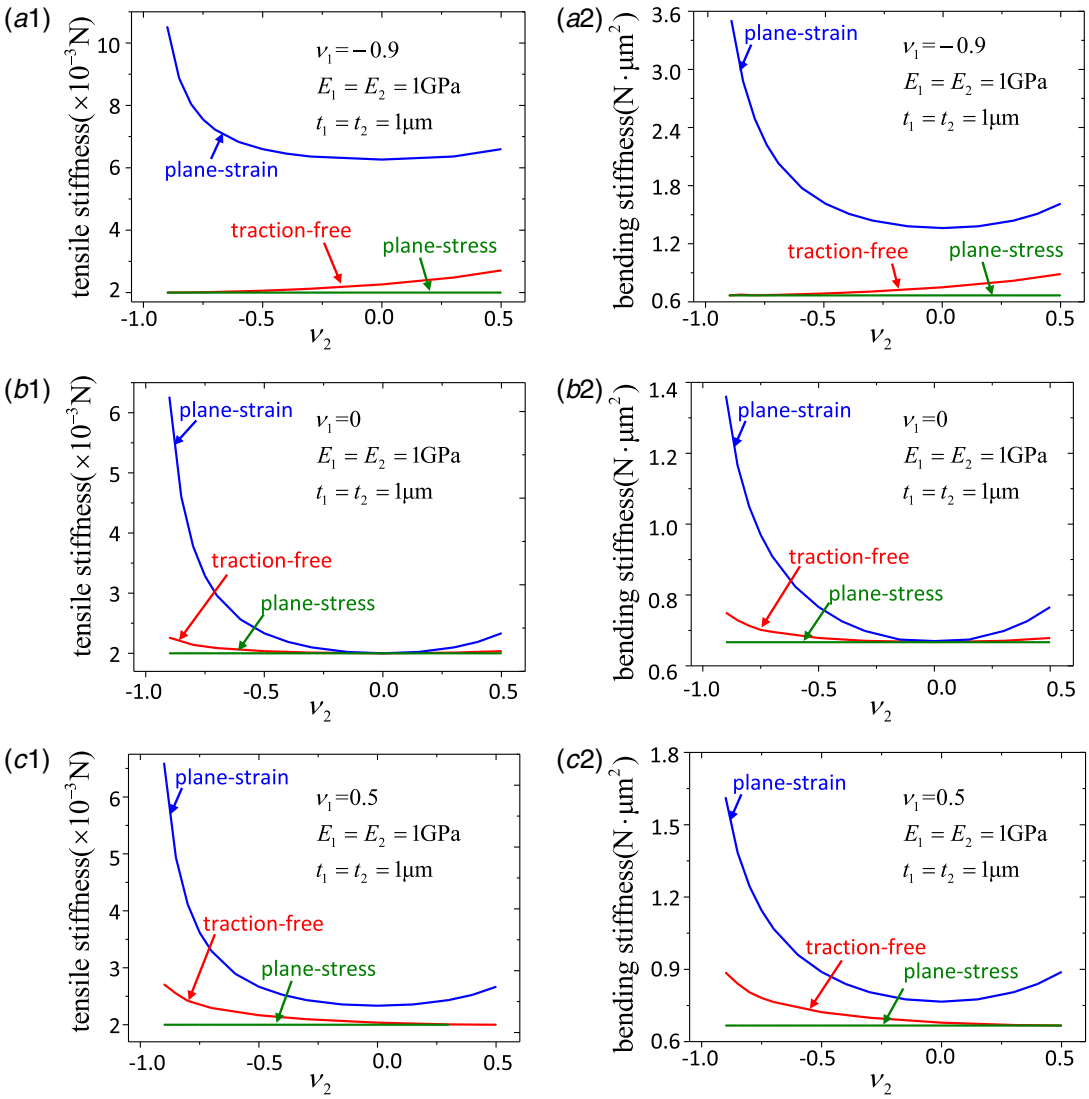

Fig. 5 The effects of Poisson's ratio ν_2 on the tensile/bending stiffness of the double-layer ribbon: (*a*1) $\nu_1 = -0.9$ for tensile stiffness, (*a*2) $\nu_1 = -0.9$ for bending stiffness, (*b*1) $\nu_1 = 0$ for tensile stiffness, (*b*2) $\nu_1 = 0$ for bending stiffness, (*c*1) $\nu_1 = 0.5$ for tensile stiffness, and (*c*2) $\nu_1 = 0.5$ for bending stiffness

beginning and becomes constant when w is large. For the extreme case with $\nu_1 = -0.9$ and $\nu_2 = 0.49$, the peaks of the shear stress becomes much larger as depicted in Fig. 4(*c*) because the deformation of the two layers becomes more uncoordinated.

Furthermore, the effects of mechanical property and geometry on the tensile/bending stiffness are also discussed for the three analytical models. Firstly, the effect of Poisson's ratio is studied as shown in Fig. 5. For the given Poisson's ratio $\nu_1 = -0.9$, 0, and 0.5, respectively, the tensile/bending stiffness as a function of ν_2 is compared with those of the three models. The result of the plane-stress model is independent of Poisson's ratio ν_1 and ν_2. For $\nu_1 = -0.9$, the tensile/bending stiffness of the plane-strain model is much larger than that of the traction-free model and the plane-stress model (Figs. 5(*a*1) and 5(*a*2)). The result of the traction-free model approaches that of the plane-stress model for $\nu_1 = \nu_2 = -0.9$ (Figs. 5(*a*1) and 5(*a*2)) and $\nu_1 = \nu_2 = 0.5$ (Figs. 5(*c*1) and 5(*c*2)), respectively. For $\nu_1 = 0$ as shown in Figs. 5(*b*1) and 5(*b*2), the results of the three models approach each other for $\nu_2 = 0$. The effects of Young's modulus E_2 and thickness t_2 are also studied in Fig. 6. The tensile/bending stiffness here is normalized by that of the plane-stress model. The results confirmed that the traction-free model can give an accurate prediction of the tensile/bending stiffness for laminated ribbons of flexible electronics, while those from the plane-strain model and the plane-stress model are not good enough.

4 Concluding Remarks

(1) The effective tensile/bending stiffness of laminated ribbons, which is frequently used as the fundamental parameter in the mechanical analysis of flexible electronics, is usually obtained by the plane-strain hypothesis for simplicity. It is found that the practical condition is usually closer to the traction free instead of the plane strain, even for the cases with a relatively large width.

(2) A traction-free model is proposed to study the effective tensile/bending stiffness of the laminated ribbon. Analytic expressions for the effective tensile/bending stiffness are obtained, which can be used directly in the mechanical analysis of flexible electronics.

(3) The prediction of the traction-free model agrees very well with the precise result, which is obtained by 3D FEA for the cases in the range of structure designs of flexible electronics. It shows the validation of the application of the traction-free model to flexible electronics.

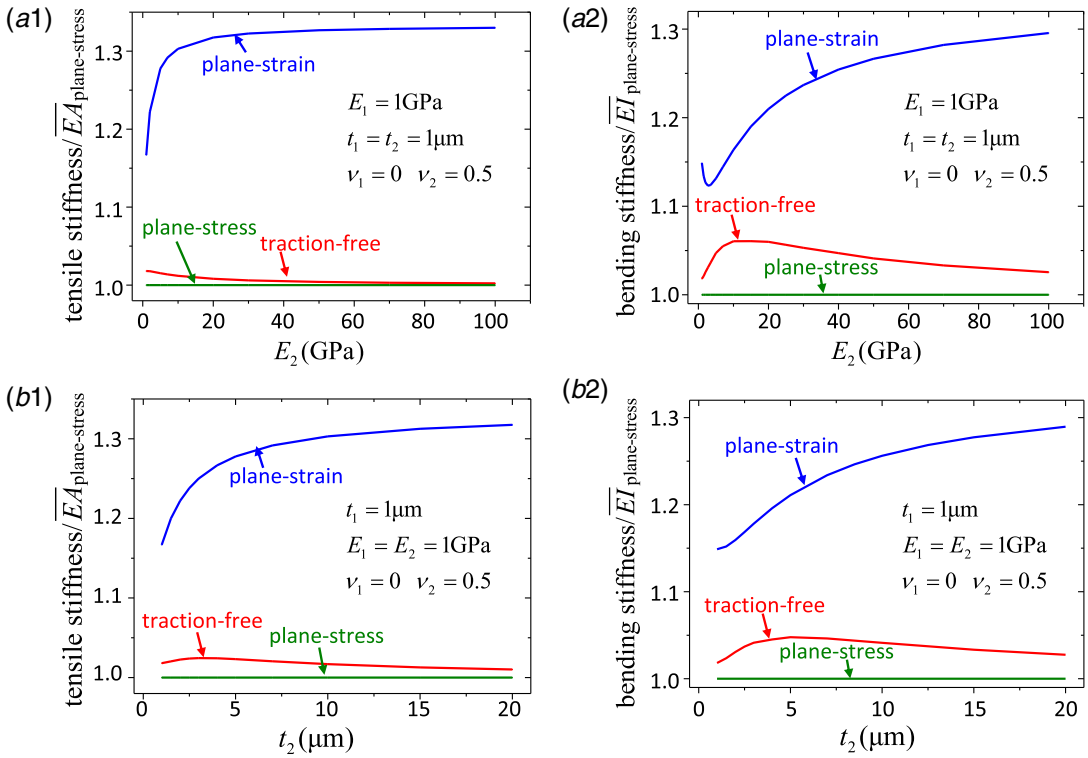

Fig. 6 The effects of Young's modulus E_2 and thickness t_2 on the tensile/bending stiffness of the double-layer ribbon: (*a*1) E_2 on tensile stiffness, (*a*2) E_2 on bending stiffness, (*b*1) t_2 on tensile stiffness, and (*b*2) t_2 on bending stiffness

(4) For all the cases we have studied, the result of the traction-free model is between the plane-stress model and the plane-strain model, but is closer to the plane-stress model. The use of the plane-strain model sometimes may yield considerable error in the mechanical analysis of flexible electronics.
(5) Effects of Poisson's ratio, Young's modulus, and the ribbon thickness are studied systematically. It shows that this work is very important for the problems with advanced materials, such as metamaterials with a negative Poisson's ratio.

Acknowledgment

The authors gratefully acknowledge the support from the National Natural Science Foundation of China (grants 11772331 and 11572323), Chinese Academy of Sciences via the "Hundred Talent Program", and Strategic Priority Research Program of the Chinese Academy of Sciences (No. XDB22040501).

References

[1] Rogers, J. A., Someya, T., and Huang, Y., 2010, "Materials and Mechanics for Stretchable Electronics," Science, **327**(5973), pp. 1603–1607.
[2] Hu, J., Li, R., Liu, Y., and Su, Y., 2018, "An Overview of Healthcare Monitoring by Flexible Electronics," Sci. China Phys. Mech., **61**(9), 094601.
[3] Ko, H. C., Stoykovich, M. P., Song, J., Malyarchuk, V., Choi, W. M., Yu, C.-J., Geddes, JB, III, Xiao, J., Wang, S., Huang, Y., and Rogers, J. A., 2008, "A Hemispherical Electronic Eye Camera Based on Compressible Silicon Optoelectronics," Nature, **454**(7205), pp. 748–753.
[4] Wagner, S., Lacour, S. P., Jones, J., Hsu, P.-h. I., Sturm, J. C., Li, T., and Suo, Z., 2004, "Electronic Skin: Architecture and Components," Physica E Low Dimens. Syst. Nanostruct., **25**(2–3), pp. 326–334.
[5] Hammock, M. L., Chortos, A., Tee, B. C., Tok, J. B., and Bao, Z., 2013, "25th Anniversary Article: The Evolution of Electronic Skin (e-Skin): A Brief History, Design Considerations, and Recent Progress," Adv. Mater., **25**(42), pp. 5997–6038.
[6] Kim, D. H., Lu, N. S., Ma, R., Kim, Y. S., Kim, R. H., Wang, S. D., Wu, J., Won, S. M., Tao, H., Islam, A., Yu, K. J., Kim, T. I., Chowdhury, R., Ying, M., Xu, L. Z., Li, M., Chung, H. J., Keum, H., McCormick, M., Liu, P., Zhang, Y. W., Omenetto, F. G., Huang, Y. G., Coleman, T., and Rogers, J. A., 2011, "Epidermal Electronics," Science, **333**(6044), pp. 838–843.
[7] Jang, K.-I., Li, K., Chung, H. U., Xu, S., Jung, H. N., Yang, Y., Kwak, J. W., Jung, H. H., Song, J., Yang, C., Wang, A., Liu, Z., Lee, J. Y., Kim, B. H., Kim, J.-H., Lee, J., Yu, Y., Kim, B. J., Jang, H., Yu, K. J., Kim, J., Lee, J. W., Jeong, J.-W., Song, Y. M., Huang, Y., Zhang, Y., and Rogers, J. A., 2017, "Self-Assembled Three Dimensional Network Designs for Soft Electronics," Nat. Commun., **8**, 15894.
[8] Kim, D. H., Wang, S., Keum, H., Ghaffari, R., Kim, Y. S., Tao, H., Panilaitis, B., Li, M., Kang, Z., Omenetto, F., Huang, Y., and Rogers, J. A., 2012, "Thin, Flexible Sensors and Actuators as 'Instrumented' Surgical Sutures for Targeted Wound Monitoring and Therapy," Small, **8**(21), pp. 3263–3268.
[9] Dagdeviren, C., Su, Y. W., Joe, P., Yona, R., Liu, Y. H., Kim, Y. S., Huang, Y. A., Damadoran, A. R., Xia, J., Martin, L. W., Huang, Y. G., and Rogers, J. A., 2014, "Conformable Amplified Lead Zirconate Titanate Sensors with Enhanced Piezoelectric Response for Cutaneous Pressure Monitoring," Nat. Commun., **5**, 4496.
[10] Fan, J. A., Yeo, W.-H., Su, Y., Hattori, Y., Lee, W., Jung, S.-Y., Zhang, Y., Liu, Z., Cheng, H., Falgout, L., Bajema, M., Coleman, T., Gregoire, D., Larsen, R. J., Huang, Y., and Rogers, J. A., 2014, "Fractal Design Concepts for Stretchable Electronics," Nat. Commun., **5**, 3266.
[11] Xu, S., Zhang, Y., Cho, J., Lee, J., Huang, X., Jia, L., Fan, J. A., Su, Y., Su, J., Zhang, H., Cheng, H., Lu, B., Yu, C., Chuang, C., Kim, T.-i., Song, T., Shigeta, K., Kang, S., Dagdeviren, C., Petrov, I., Braun, P. V., Huang, Y., Paik, U., and Rogers, J. A., 2013, "Stretchable Batteries With Self-Similar Serpentine Interconnects and Integrated Wireless Recharging Systems," Nat. Commun., **4**, 1543.
[12] Su, Y., Liu, Z., and Xu, L., 2016, "An Universal and Easy-to-Use Model for the Pressure of Arbitrary-Shape 3D Multifunctional Integumentary Cardiac Membranes," Adv. Healthcare Mater., **5**(8), pp. 889–892.
[13] Xu, L., Gutbrod, S. R., Bonifas, A. P., Su, Y., Sulkin, M. S., Lu, N., Chung, H.-J., Jang, K.-I., Liu, Z., Ying, M., Lu, C., Webb, R. C., Kim, J.-S., Laughner, J. I., Cheng, H., Liu, Y., Ameen, A., Jeong, J.-W., Kim, G.-T., Huang, Y., Efimov, I. R., and Rogers, J. A., 2014, "3D Multifunctional Integumentary Membranes for Spatiotemporal Cardiac Measurements and Stimulation Across the Entire Epicardium," Nat. Commun. **5**, p. 3329.
[14] Dagdeviren, C., Yang, B. D., Su, Y. W., Tran, P. L., Joe, P., Anderson, E., Xia, J., Doraiswamy, V., Dehdashti, B., Feng, X., Lu, B. W., Poston, R., Khalpey, Z., Ghaffari, R., Huang, Y. G., Slepian, M. J., and Rogers, J. A., 2014, "Conformal Piezoelectric Energy Harvesting and Storage From Motions of the Heart, Lung, and Diaphragm," Proc. Natl. Acad. Sci. U.S.A., **111**(5), pp. 1927–1932.
[15] Su, Y. W., Dagdeviren, C., and Li, R., 2015, "Measured Output Voltages of Piezoelectric Devices Depend on the Resistance of Voltmeter," Adv. Funct. Mater., **25**(33), pp. 5320–5325.

[16] Su, Y. W., Li, S. A., Li, R., and Dagdeviren, C., 2015, "Splitting of Neutral Mechanical Plane of Conformal, Multilayer Piezoelectric Mechanical Energy Harvester," Appl. Phys. Lett., **107**(4), 1905.
[17] Dagdeviren, C., Hwang, S.-W., Su, Y., Kim, S., Cheng, H., Gur, O., Haney, R., Omenetto, F. G., Huang, Y., and Rogers, J. A., 2013, "Transient, Biocompatible Electronics and Energy Harvesters Based on ZnO," Small, **9**(20), pp. 3398–3404.
[18] Li, S., Liu, X., Li, R., and Su, Y., 2017, "Shear Deformation Dominates in the Soft Adhesive Layers of the Laminated Structure of Flexible Electronics," Int. J. Solids Struct., **110**, pp. 305–314.
[19] Liu, H., Zhao, H., Li, S., Hu, J., Zheng, X., Li, R., Chen, Y., and Su, Y., 2018, "Adhesion-Free Thin-Film-Like Curvature Sensors Integrated on Flexible and Wearable Electronics for Monitoring Bending of Joints and Various Body Gestures," Adv. Mater. Technol., **4**, 1800327.
[20] Su, Y., Ping, X., Yu, K. J., Lee, J. W., Fan, J. A., Wang, B., Li, M., Li, R., Harburg, D. V., Huang, Y., Yu, C., Mao, S., Shim, J., Yang, Q., Lee, P. Y., Armonas, A., Choi, K. J., Yang, Y., Paik, U., Chang, T., Dawidczyk, T. J., Huang, Y., Wang, S., and Rogers, J. A., 2017, "In-Plane Deformation Mechanics for Highly Stretchable Electronics," Adv. Mater., **29**(8), 1604989.
[21] Lee, Y. K., Jang, K.-I., Ma, Y., Koh, A., Chen, H., Jung, H. N., Kim, Y., Kwak, J. W., Wang, L., Xue, Y., Yang, Y., Tian, W., Jiang, Y., Zhang, Y., Feng, X., Huang, Y., and Rogers, J. A., 2017, "Chemical Sensing Systems that Utilize Soft Electronics on Thin Elastomeric Substrates with Open Cellular Designs," Adv. Funct. Mater., **27**(9), 1605476.
[22] Kim, D.-H., Ahn, J.-H., Choi, W. M., Kim, H.-S., Kim, T.-H., Song, J., Huang, Y. Y., Liu, Z., Lu, C., and Rogers, J. A., 2008, "Stretchable and Foldable Silicon Integrated Circuits," Science, **320**, pp. 507–511.
[23] Khang, D. Y., Jiang, H. Q., Huang, Y., and Rogers, J. A., 2006, "A Stretchable Form of Single-Crystal Silicon for High-Performance Electronics on Rubber Substrates," Science, **311**(5758), pp. 208–212.
[24] Su, Y., Li, R., Cheng, H., Ying, M., Bonifas, A. P., Hwang, K.-C., Rogers, J. A., and Huang, Y., 2013, "Mechanics of Finger-Tip Electronics," J. Appl. Phys., **114**(16), 164511.
[25] Wang, S., Li, M., Wu, J., Kim, D.-H., Lu, N., Su, Y., Kang, Z., Huang, Y., and Rogers, J. A., 2012, "Mechanics of Epidermal Electronics," ASME J. Appl. Mech. Trans., **79**(3), 031022.
[26] Su, Y., Wu, J., Fan, Z., Hwang, K.-C., Song, J., Huang, Y., and Rogers, J. A., 2012, "Postbuckling Analysis and its Application to Stretchable Electronics," J. Mech. Phys. Solids, **60**(3), pp. 487–508.
[27] Hwang, S.-W., Tao, H., Kim, D.-H., Cheng, H., Song, J.-K., Rill, E., Brenckle, M. A., Panilaitis, B., Won, S. M., Kim, Y.-S., Song, Y. M., Yu, K. J., Ameen, A., Li, R., Su, Y., Yang, M., Kaplan, D. L., Zakin, M. R., Slepian, M. J., Huang, Y., Omenetto, F. G., and Rogers, J. A., 2012, "A Physically Transient Form of Silicon Electronics," Science, **337**(6102), pp. 1640–1644.
[28] Song, J., 2015, "Mechanics of Stretchable Electronics," Curr. Opin. Solid State Mater. Sci., **19**(3), pp. 160–170.
[29] Zhang, Y., Huang, Y., and Rogers, J. A., 2015, "Mechanics of Stretchable Batteries and Supercapacitors," Curr. Opin. Solid State Mater. Sci., **19**(3), pp. 190–199.
[30] Song, J., Feng, X., and Huang, Y., 2016, "Mechanics and Thermal Management of Stretchable Inorganic Electronics," Natl. Sci. Rev., **3**(1), pp. 128.
[31] Jiang, H., Khang, D.-Y., Fei, H., Kim, H., Huang, Y., Xiao, J., and Rogers, J. A., 2008, "Finite Width Effect of Thin-Films Buckling on Compliant Substrate: Experimental and Theoretical Studies," J. Mech. Phys. Solids, **56**(8), pp. 2585–2598.
[32] Song, J., Jiang, H., Liu, Z. J., Khang, D. Y., Huang, Y., Rogers, J. A., Lu, C., and Koh, C. G., 2008, "Buckling of a Stiff Thin Film on a Compliant Substrate in Large Deformation," Int. J. Solids Struct., **45**(10), pp. 3107–3121.
[33] Kim, D. H., Liu, Z., Kim, Y. S., Wu, J., Song, J., Kim, H. S., Huang, Y., Hwang, K. C., Zhang, Y., and Rogers, J. A., 2009, "Optimized Structural Designs for Stretchable Silicon Integrated Circuits," Small, **5**(24), pp. 2841–2847.
[34] Vanfleteren, J., Gonzalez, M., Bossuyt, F., Hsu, Y. Y., Vervust, T., De Wolf, I., and Jablonski, M., 2012, "Printed Circuit Board Technology Inspired Stretchable Circuits," MRS Bull., **37**(03), pp. 254–260.
[35] Jahanshahi, A., Gonzalez, M., Brand, J. v. d., Bossuyt, F., Vervust, T., Verplancke, R., Vanfleteren, J., and Baets, J. D., 2013, "Stretchable Circuits with Horseshoe Shaped Conductors Embedded in Elastic Polymers," Jpn. J. Appl. Phys., **52**(5S1), 05DA18.
[36] Lee, C. H., Jeong, J.-W., Liu, Y., Zhang, Y., Shi, Y., Kang, S.-K., Kim, J., Kim, J. S., Lee, N. Y., Kim, B. H., Jang, K.-I., Yin, L., Kim, M. K., Banks, A., Paik, U., Huang, Y., and Rogers, J. A., 2015, "Materials and Wireless Microfluidic Systems for Electronics Capable of Chemical Dissolution on Demand," Adv. Funct. Mater., **25**(9), pp. 1338–1343.
[37] Su, Y., Wang, S., Huang, Y., Luan, H., Dong, W., Fan, J. A., Yang, Q., Rogers, J. A., and Huang, Y., 2015, "Elasticity of Fractal Inspired Interconnects," Small, **11**(3), pp. 367–373.
[38] Xu, S., Yan, Z., Jang, K.-I., Huang, W., Fu, H., Kim, J., Wei, Z., Flavin, M., McCracken, J., Wang, R., Badea, A., Liu, Y., Xiao, D., Zhou, G., Lee, J., Chung, H. U., Cheng, H., Ren, W., Banks, A., Li, X., Paik, U., Nuzzo, R. G., Huang, Y., Zhang, Y., and Rogers, J. A., 2015, "Assembly of Micro/Nanomaterials Into Complex, Three-Dimensional Architectures by Compressive Buckling," Science, **347**(6218), pp. 154–159.
[39] Kim, D. H., Song, J., Choi, W. M., Kim, H. S., Kim, R. H., Liu, Z., Huang, Y. Y., Hwang, K. C., Zhang, Y. W., and Rogers, J. A., 2008, "Materials and Noncoplanar Mesh Designs for Integrated Circuits With Linear Elastic Responses to Extreme Mechanical Deformations," Proc. Natl. Acad. Sci. U.S.A., **105**(48), pp. 18675–18680.
[40] Lee, J., Wu, J., Shi, M., Yoon, J., Park, S. I., Li, M., Liu, Z., Huang, Y., and Rogers, J. A., 2011, "Stretchable GaAs Photovoltaics With Designs That Enable High Areal Coverage," Adv. Mater., **23**(8), pp. 986–991.
[41] Shin, G., Jung, I., Malyarchuk, V., Song, J., Wang, S., Ko, H. C., Huang, Y., Ha, J. S., and Rogers, J. A., 2010, "Micromechanics and Advanced Designs for Curved Photodetector Arrays in Hemispherical Electronic-Eye Cameras," Small, **6**(7), pp. 851–856.
[42] Wu, J., Liu, Z. J., Song, J., Huang, Y., Hwang, K. C., Zhang, Y. W., and Rogers, J. A., 2011, "Stretchability of Encapsulated Electronics," Appl. Phys. Lett., **99**(6), 061911.
[43] Lan, L., Lin, H., Qiao, S., Yi, Z., Danto, S., Richardson, K., Musgraves, J. D., Lu, N., and Hu, J., 2014, "Integrated Flexible Chalcogenide Glass Photonic Devices," Nat. Photonics, **8**(8), pp. 643–649.
[44] MingLi, J., JianWu, R.-H., ZhanKang, Y., and Rogers, J., 2010, "Mechanics Analysis of Two-Dimensionally Prestrained Elastomeric Thin Film for Stretchable Electronics," Acta Mech. Solida Sinica, **23**(6), pp. 592–599.
[45] Dassault-Systèmes, 2010, *Abaqus Analysis User's Manual v.6.10*, Dassault Systèmes Simulia Corp., Providence, RI.